Journal of
Materials Chemistry A

Materials for energy and sustainability

Accepted Manuscript

This article can be cited before page numbers have been issued, to do this please use: M. L. Aubrey, A. Wang, R. S. Storteboom, S. S. Mollick and S. Vasylevskyi, *J. Mater. Chem. A*, 2026, DOI: 10.1039/D5TA09290F.

ROYAL SOCIETY OF CHEMISTRY

rsc.li/materials-a

View Article Online
DOI: 10.1039/D5TA09290F

Calcium Pyrenide: A Room-Temperature Reagent for Stoichiometric Calciations and Reductive Ca^{2+} Intercalation Reactions

Anda Wang[†,1], Ryan S. Storteboom[†,1], Shain Sagar Mollick[†], Serhii Vasylevskyi[†], Michael L. Aubrey[†,*]

[†]Department of Chemistry, The University of Texas at Austin, Austin, TX 78712, USA.
[1]Authors contributed equally

ABSTRACT: Chemical reductive insertion of metal ions using metal arenes has attracted significant attention due to its capability to readily modulate the electronic and structural properties of host materials. Despite extensive studies involving various metal arenes, systems capable of enabling reductive insertion with Ca^{2+} species have not been determined. Here, we report the synthesis of calcium pyrenide and demonstrate its effectiveness in facilitating reductive insertion into host frameworks. The nominal composition in solution was determined to be spectroscopically consistent with previously reported alkali metal pyrenide solutions and, in DMF, found to participate in stoichiometric titrations of silver salts. Single crystals were grown from THF solutions and structurally characterized by X-ray diffraction. Signatures of the pyrenide's radical anion were observed by EPR. The reduction potential was estimated by cyclic voltammetry of pyrene in a calcium perchlorate electrolyte solution where a reversible one-electron reduction wave was observed at –2.52 V vs Fc/Fc^+. To demonstrate the utility of $Ca(pyrene)_2$ for screening materials capable of reversible calciation via reductive intercalation, the compounds, $Ca_x(DMF)_yMoS_2$ ($0 < x < 0.34$) were prepared from DMF solutions of calcium pyrenide and characterized by PXRD, SEM, ICP-OES, and TGA.

■ INTRODUCTION

Reductive insertion involves the electronation of a host crystal structure and migration of a cation into the host for charge balance. Reductive insertion reactions—termed reductive intercalation reactions for layered host crystals—have found many applications, most prominently as electrode materials for lithium-ion batteries.[1–3] The insertion of alkali metals has also been shown to induce diverse changes in the electronic properties of materials, including changes in electron transport, switching between conducting and insulating phases, and the emergence of new magnetic and superconducting phases.[4–6]

The more recent emergence of materials capable of reductive insertion of multivalent cations offers the possibility of accessing novel structural and electronic phase transitions distinct from analogous monovalent ion insertion reactions. This is due to the higher charge densities and stronger interactions of divalent cations with a host lattice.[7,8] These interactions may result in stronger coupling between multiple polaronic carriers associated with a single inserted cation,[9] and their divalent character may allow inclusion of magnetic or redox-active cations, which are rare among common monovalent cations. However, the emerging set of materials known to reversibly insert divalent cations is minuscule in comparison to those hosts capable of supporting reversible monovalent ion insertion. This is in large part due to the high charge density of 2+ cations greatly reducing their diffusivities in the solid state, but also in part due to a lack of suitable chemical and electrochemical reduction conditions that are broadly applicable to a wide range of materials. The development of easily accessible, low-cost chemical reductants would allow for facile reaction screening under a consistent set of reaction conditions and may accelerate the discovery of new multivalent ion insertion materials.

Calcium has a low reduction potential (–2.87 V vs SHE), global abundance, and relatively low cost, making it a promising option for low-cost energy storage applications.[10] To varying extents, electrochemical Ca^{2+} insertion has been investigated in host materials, including α-V_2O_5, α-MoO_3, $CaCo_2O_4$, MoS_2 , TiS_2, $NaV_2(PO_4)_3$, and Prussian-blue analogues.[11–17] Generally, electrochemical methods present some limitations: (1) the active materials are typically embedded in a carbon composite, which prevents isolation and characterization of phase-pure products; (2) the quantity of product that can be prepared electrochemically is often small and difficult to scale; and (3) constructing electrochemical cells takes longer and is less parallelizable than solution-phase chemical reductions.

Existing chemical insertion strategies for Ca^{2+} include dissolution of Ca in ammonia.[14] This method requires reaction temperatures below –34 °C to maintain liquid ammonia, and involves the use of toxic NH_3 (g). CaI_2 has also been used as a reductant to reduce $NaV_2(PO_4)_3$ at 150 °C.[12] Iodide is a weak reductant and potentially coordinating ligand. These limitations motivated a search for an alternative reductant with a lower reduction potential that could be used at room temperature with minimal byproducts.

Metal arene complexes are well known effective reductants for the chemical insertion of metal cations into host materials.[18] These complexes are typically synthesized by reacting an arene with an alkali or alkaline earth metal in solution, resulting in a binary salt of a persistent arene radical anion. Metal arenides are strong reductants and yield only non-coordinating hydrocarbons upon oxidation, making them attractive for clean redox chemistry where reduced solids can be readily isolated and purified by filtration.[18] For example, binary arene salts of Li^+, Na^+, K^+, and Mg^{2+} in combination with naphthalene, anthracene, and pyrene have been employed in many reductive insertion reactions.[19–26] However, to our knowledge, calcium arenides suitable for use as stoichiometric reductants have not been isolated.

We report the formation of a calcium pyrenide salt and the isolation of its co-crystal with pyrene $Ca(THF)_6(pyrene)_2(pyrenide^{\bullet-})_2$. Calcium pyrenides are shown to participate in stoichiometric chemical reductions, including

View Article Online
DOI: 10.1039/D5TA09290F

the reductive insertion of Ca^{2+} into MoS_2 in DMF solutions. Described are recommended procedures for the preparation of calcium pyrenide solutions for use as reagents for chemical reductions.

EXPERIMENTAL

General Methods. Pyrene (98%, Thermo Scientific Chemicals), 1,2-dibromoethane (98%, Thermo Scientific Chemicals), and molybdenum(IV) sulfide (98%, Sigma Aldrich) were used as received without further purification. N,N-Dimethylformamide (Certified ACS, Thermo Scientific Chemicals) was stored over 4 Å molecular sieves for three days, degassed by three 'freeze-pump-thaw' cycles, then stored in a N_2 glovebox. THF (>95%, Fisher Scientific) and hexanes (>96%, TCI America) were column-dried using a solvent purification system designed by Innovative Technologies and stored over 4 Å molecular sieves in a N_2 glovebox. Ferrocene (98%, Acros Organics) was recrystallized by sublimation and condensation. Anhydrous calcium perchlorate was prepared using calcium perchlorate tetrahydrate (99%, Sigma Aldrich) vacuum dried at 180 °C under flowing N_2 for 24 hours at 50 mTorr and confirmed by the absence of water peaks in FT-IR. Calcium turnings (99 %, Sigma Aldrich) were washed with a mixture containing a trace amount of pyrene in DMF and dried by rinsing with DMF followed by THF. Molecular sieves were vacuum dried at 220 °C under flowing N_2 for 24 hours at 50 mTorr. DME (Sigma-Aldrich) was purified by distillation over sodium benzophenone and stored over 4 Å molecular sieves in an N_2 glovebox.

Material Characterization. Powder X-ray diffraction (PXRD) pattern were collected using a Rigaku II Miniflex G6 equipped with a 600 W Cu Kα source, a 0.5° Soller slit, and a Hypix-400MF hybrid pixel array detector. Air-free PXRD was collected using a Rigaku R-Axis Spider diffractometer (40 kV and 40 mA) equipped with a Cu Kα source (λ = 1.5418 Å). EPR was collected using a Bruker Biospin EMXplus 114 X-band spectrometer equipped with a liquid nitrogen cryostat. UV-*vis* spectroscopy was collected using a PerkinElmer Lambda 365. Morphology and elemental mapping of $Ca_x(DMF)_yMoS_2$ were obtained using an Apreo2C loVac and FEI Quanta 650 ESEM. Inductively coupled plasma optical emission spectroscopy (ICP-OES) was collected using an Agilent 5800 and Agilent SPS 4 Autosampler in the Department of Civil, Architectural and Environmental Engineering at the University of Texas at Austin. Thermogravimetric analysis (TGA) was performed on a TA Instruments Q50 analyzer using high purity N_2 carrier gas in the range of 25 – 800 °C. A ramp rate of 5 °C min^{-1} and a N_2 flow rate of 50 mL min^{-1} were applied between 25 °C and 800 °C.

Single crystal X-ray diffraction. Single crystal X-ray diffraction was conducted using a Rigaku XtaLAB Synergy equipped with a Hypix hybrid pixel array detector. The data were collected at 100 K using a PhotonJet micro-focus Cu-Kα radiation source (λ = 1.54184 Å). Data collection, unit cell refinement, and data reduction were performed using Rigaku Oxford Diffraction's CrysAlisPro V 1.171.40.53. The structure was solved by direct methods using SHELXT[27] and refined by full-matrix least-squares on F^2 with anisotropic displacement parameters for the non-hydrogen atoms using SHELXL-2019/3 running under the OLEX2 graphical interface.[28,29] Structures were visualized using VESTA.[30]

Electrochemical Measurements. Cyclic voltammetry was performed using a Bio-Logic VSP-3e 8-channel multipotentiostat under nitrogen in a 30 mL jar, with a cap fitted with a glassy carbon working electrode, platinum wire counter electrode, and silver / silver nitrate reference electrode. The active surface of the glassy carbon working electrode is a circle with an area of 0.222 cm^2. The electrodes were submersed in a dry, degassed DMF solution containing 1 mM pyrene, 1 mM ferrocene, and 100 mM of either $NaClO_4$ or $Ca(ClO_4)_2$.

Synthesis of calcium pyrenide. Calcium turnings (40 mg, 1 mmol) and pyrene (424 mg, 2.1 mmol) were mixed in DMF (3956 mg) in an N_2-filled glovebox separately. 1,2-dibromoethane (236 mg, 1.26 mmol) was diluted by DMF (9436 mg). The diluted 1,2-dibromoethane solution (77 mg solution, 1.88 mg DBE, 0.01 mmol) was added into the reaction mixture. Bright blue chemiluminescence was observed when the mixture started to stir. After photoemission ceased, the solution quickly turned an opaque dark orange color. The solution was then stirred at room temperature for an additional 2 h, yielding a dark red solution.

To prolong the chemiluminescent reaction and slow product formation, as shown in **Supplementary Video S1**, the same reagents in the quantities (1113 mg, 5.509 mmol) of pyrene, (77 mg, 1.925 mmol) calcium ingot, and 5 mol% 1,2-dibromoethane in 12 mL of DMF were used.

Titration of calcium pyrenide solutions by Ag deposition. $AgPF_6$ (556 mg, 2.2 mmol) was reacted with calcium pyrenide (444 mg, 1 mmol), which was filtered through glass wool in a pre-weighed 20 mL vial. After 1 hour, the mixture was centrifuged. The solvent was decanted and refilled with DMF. The mixture was sonicated for 5 s, followed by centrifuging and again decanting the solvent. A second wash was conducted using THF. The vial was vacuum dried for 12 h and the vial was reweighed.

Synthesis of $Ca(THF)_6(pyrene)_2(pyrenide^{\bullet-})_2$ single crystals. Excess calcium turnings, pyrene (200 mg, 0.99 mmol), and 1,2-dibromoethane (25 mg, 0.13 mmol) were mixed in THF in a N_2 filled glovebox. The solution turned dark red after 12 h. This solution was then placed under vacuum until all the solvent was evaporated and only the red precipitate remained. Using a minimal amount of THF, the red solid was redissolved and recrystallized by vapor diffusion of hexanes at –24 °C. Data for the refined crystal structure were deposited in the Cambridge Structural Database (CSD) with deposition number 2489905. A plot of the asymmetric unit and a table of associated crystallographic data are provided in **Supplementary Figure S1 and Table S1**.

Synthesis of $Ca_x(DMF)_yMoS_2$. In an N_2-filled glovebox, calcium turnings (49 mg, 1.23 mmol), pyrene (519 mg, 2.58 mmol), and 1,2-dibromoethane (2.3 mg, 0.012 mmol) were added to a 20-ml borosilicate glass scintillation vial. The mixture was stirred at room temperature for 4 h, then 0.3, 0.5, and 0.7 equivalents of $Ca(pyrene)_2$ (*Solv*, DMF) were added into MoS_2. The mixture was stirred for 24 hours; the product was filtered and washed with DMF and THF in an N_2-filled glovebox. The black powder product was characterized by SEM and PXRD. The chemical composition of the inserted product was determined by EDX, ICP-OES, and TGA.

RESULTS AND DISCUSSION

Calcium pyrenide in DMF was prepared by first activating calcium metal with 1,2-dibromoethane in DMF, then adding

View Article Online
DOI: 10.1039/D5TA09290F

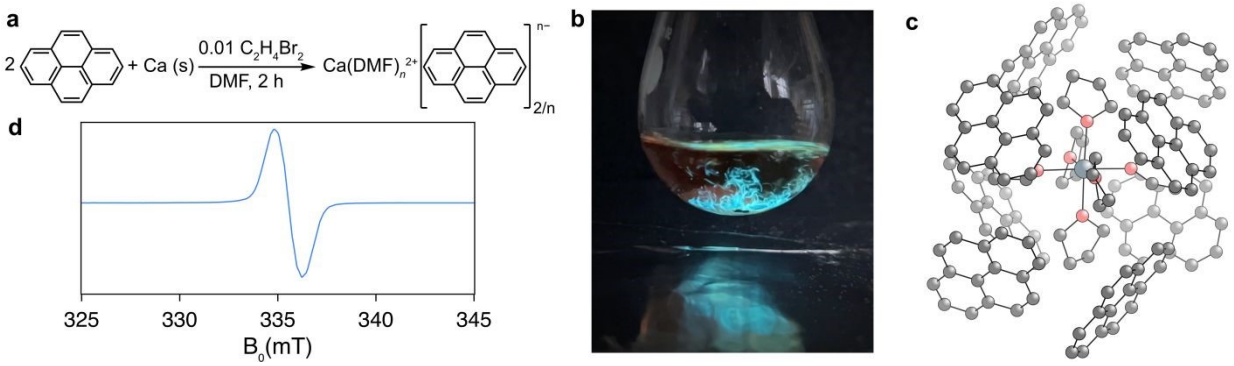

Figure 1. Reaction scheme for the formation of calcium pyrenide (a). Photograph depicting the chemiluminescent stage of the reaction in DMF (b). Portion of a single crystal structure of $Ca(THF)_6(pyrene)_2(pyrenide^{\bullet-})_2$. Carbon, oxygen, and calcium are shown in grey, red, and slate-grey, respectively. Modeled hydrogen positions are omitted for clarity (c). X-band EPR spectrum of calcium pyrenide in DMF collected at 100 K (d).

two equivalents of pyrene while stirring at room temperature, **Figure 1a**. Following the addition of pyrene, a bright blue chemiluminescent emission appeared as product diffused from the calcium surface, **Figure 1b and Supplementary Video S1**. The participation of pyrenide in chemiluminescence has been documented in other contexts and attributed to the oxidation of pyrenides—here by 1,2-dibromoethane and its decomposition products—to form the neutral pyrene excimer ultimately responsible for the observed emission. Similar mechanisms were proposed to explain the chemiluminescence and electrochemiluminescence of arenides, including pyrene, as early as 1967.[31,32] Only after chemiluminescence ceased did the reaction mixture gradually develop an orange coloration, transitioning to a dark red after stirring for 1–2 hours. This color transition is consistent with that of pyrenide's sodium salt in solution. Qualitatively, this formation of reduced pyrenes can be delayed by increasing either the concentration of pyrene or the concentration of 1,2-dibromoethane. Slow desorption of pyrene/pyrenide from the calcium surface may explain the negative reaction order for pyrene. Excess 1,2-dibromoethane that does not decompose in the activation of the calcium metal surface likely oxidizes reduced pyrenes in solution, and chemiluminescence continues until it has been depleted.

The DMF solution formed by reacting calcium with 2.1 equivalents of pyrene was titrated by the addition of 2.2 equivalents of $AgPF_6$ to stoichiometrically precipitate Ag (*s*). Gravimetric analysis of the resulting black powder confirmed two equivalents of Ag (*s*) were recovered per mole of calcium in solution. **Supplementary Figure S2** shows the PXRD of the precipitate, in which the majority phase was identified as Ag (*s*). An impurity peak at 31° matches the expected pattern of AgBr, originating from the decomposition of 1,2-dibromoethane. The estimated yield of silver was 99.5% before, and 97.8% after, accounting for the theoretical maximum inclusion of AgBr (*s*) estimated by assuming 100% of the total moles of 1,2-dibromoethane added to the reaction coprecipitated as an AgBr (s) impurity phase.

Insoluble calcium metal powder may also reduce Ag^+ and indeed when less than two equivalents of pyrene were used to form the calcium pyrenide solution, black calcium powder was recovered by vacuum filtration and confirmed by powder X-ray diffraction to be residual Ca (*s*) from the corroded ingots. In these scenarios Ag^+ reduction is also stoichiometric with respect to the quantity of Ca (*s*) reactant. Generally, the use of excess pyrene is recommended to allow complete dissolution of Ca (*s*) in DMF.

Single crystals of calcium pyrenide, with the tentative composition $Ca(THF)_6(pyrene)_2(pyrenide^{\bullet-})_2$, were grown from THF in the presence of excess pyrene by vapor diffusion of hexanes at –30 ºC, **Figure 1c**. The crystal lattice contains two neutral pyrene and two apparently reduced pyrenide anions, as indicated in **Supplementary Figure S3.** Each $Ca(THF)_6$ molecular ion in the structure is enclathrated by four pyrene and four pyrenide molecules. Average bond lengths of the central C–C bond, and its four adjacent neighbors in the tentatively assigned neutral pyrene molecules are 1.421(1) and 1.426(2) Å, respectively. These results are comparable to previously reported bond lengths in pure pyrene crystals of 1.4244(19) Å for the central C–C distance and an average of 1.418(3) Å C–C distance for the four adjacent bonds.[33] Of the four tentatively assigned pyrenide ions, two are disordered, limiting the accuracy of their estimated bond distances. For the remaining two crystallographically ordered pyrenide anions, the average central bond C–C distance is similar to pyrene at 1.425(2) Å and the four bonds adjacent to the central C–C bond are slightly longer with a distance of 1.442(12) Å. In a previously reported $Na(diglyme)_2 \cdot pyrenide$ complex,[34] the average central C–C distance was 1.424(5) Å, and the average bond distance for the four adjacent C–C bonds was 1.432(4) Å. This slight expansion of the C–C bonds observed for both the sodium salts and the calcium salt reported here is consistent with the reduction of pyrene.

The reduction of pyrene has been reported to form both a radical anion and a singlet dianion.[34–37] To evaluate the electronic states of pyrene in calcium pyrenide (*Solv*, DMF), X-band EPR spectroscopy was performed on a 25 mM calcium pyrenide solution in DMF at 100 K, **Figure 1d**. The spectrum exhibited a singlet with a g-factor of 2.0029 and unresolved hyperfine splitting, a notable distinction from the EPR spectra of electrochemically derived tetrabutylammonium salt, which display the expected hyperfine splitting and a similar g-factor of 2.0028.[36] This observation may be attributed to the calcium cation withdrawing electron density from the pyrenide radical, thereby diminishing hyperfine coupling. Alternatively, reduction products of pyrene in THF only form the singlet dianion with more electropositive metals including Li, K, and Rb and may display a broad single-line EPR signal that has been attributed to the dissolved alkali metal and its equilibrium with

View Article Online
DOI: 10.1039/D5TA09290F

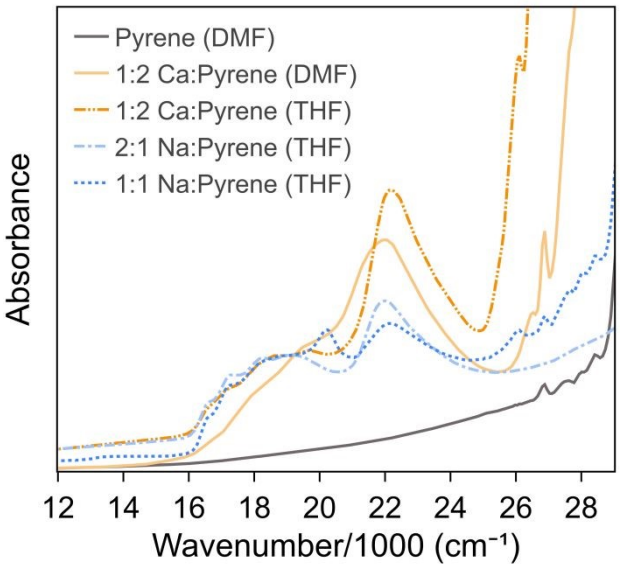

Figure 2. UV-*vis* absorption spectra of pyrene in DMF (grey, solid), a pyrene solution reacted with ½ equivalent of calcium in DMF (light orange) and THF (orange), and spectra for pyrene reacted with 2 equivalents (light blue) and 1 equivalent (blue) of sodium in THF.

electron dissolution.[35] As Ca^{2+} has a similar reduction potential to these alkali metals and the principal isotope (^{40}Ca) is similarly spinless, electron dissolution from Ca may also explain the observed EPR signal. A very similar EPR spectrum is observed for calcium pyrenide in THF solutions, **Supplementary Figure S4**.

UV-*vis* absorption spectra were collected on diluted 1:2 calcium : pyrene solutions, **Figure 2**. In DMF, a prominent absorption peak at 22,000 cm^{-1} and additional peaks at 19,600 cm^{-1}, 18,400 cm^{-1}, and 16,700 cm^{-1} were observed. Similar spectra were observed for pyrene reduced by calcium in THF solutions. The calcium spectra match the previously reported 2:1 sodium: pyrene solutions in THF assigned to the 2– oxidation state.[35] Spectrum of a 1:1 ratio of sodium to pyrene in THF did result in the emergence of a peak at 20,200 cm^{-1} consistent with the 1– oxidation state, previously observed following irradiation of 2:1 sodium: pyrene solutions in THF. Spectra of a 1:1 ratio of calcium to pyrene in DMF also did not result in the emergence or disappearance of new peaks that could be definitively assigned to a pyrene^{1-} radical anion, **Supplementary Figure S5**. Across all calcium: pyrene stoichiometries investigated, the UV-vis absorption spectra suggest pyrene is predominantly in the 2– oxidation state. At higher energies, absorption peaks consistent with charge-neutral pyrene were also observed even when excess calcium was used in the reaction.

To further explore the reduction and stoichiometry of pyrene reduction in the presence of calcium, a cyclic voltammogram of 1 mM pyrene in a 0.1 M DMF solution of calcium perchlorate was collected. A single reversible electrochemical reduction wave was observed at –2.52 V vs Fc/Fc^+, **Figure 3,** and was persistent over multiple sweeps. Sweeping to more reducing potentials in search of a second reductive wave for pyrene was limited by the electrochemical stability window of the DMF solution of calcium perchlorate used as the electrolyte, **Supplementary Figure S8**.

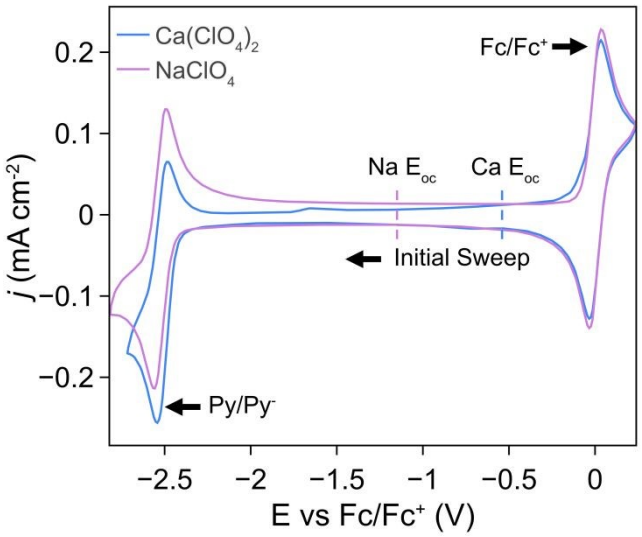

Figure 3. Cyclic voltammogram of 1mM pyrene, 1mM ferrocene, 0.1M $Ca(ClO_4)_2$ (blue) or 0.1M $NaClO_4$ (purple) in DMF collected using a glassy carbon working electrode, platinum wire counter electrode, and silver / silver nitrate reference electrode at a scan rate of 50 mV/s.

Because ferrocene is known to undergo a one-electron oxidation, 1 mM of ferrocene was also added to compare electrode kinetics. Relative to the ferrocene redox couple, the peak areas for the pyrene redox feature were approximately the same integrated area, indicating consistency with pyrene also undergoing a one-electron redox process. This is consistent with previous reports of electrochemical reduction of pyrene yielding the radical anions in THF solutions of tetrabutylammonium hexafluorophosphate that were identified by *in situ* EPR.[36,37] Both electrochemical systems were measured at a variety of scan rates to gain insight into the electrode kinetics, **Supplementary Figures S9 and S12**. Peak separations for both Fc^+/Fc and Py/Py^- waves are about 68 mV at 25 mV/s, and peak separations for both waves gradually increase with scan rate up to 800 mV/s, suggesting that they have similar electron-transfer kinetics. For the Fc^+/Fc wave, this deviation from ideality is due to slow ferrocenium adsorption kinetics.[38,39] Likewise, the Py/Py^- wave deviated from ideality due to slow pyrene/pyrenide desorption from the electrode (**Supplementary Tables S2 and S3)**. Peak currents for both Fc^+/Fc and Py/Py^- increase linearly with the square root of the scan rate suggestive of a diffusion-limited process **(Supplementary Figures S10–S14)**.

Reductive Intercalation of Ca^{2+}. To evaluate calcium pyrenide's use in screening for materials capable of undergoing reversible intercalation/insertion of calcium, powder samples of 2H-MoS_2 were identified as candidate intercalation solids. The reductive intercalation of monovalent cations into 2H-MoS_2 is well known[40] and commonly used to induce its transition to the 1T phase as well as to mediate its exfoliation to yield 2D sheets and ultrathin nanocrystals via forced hydration.[41–43] The reductive intercalation of calcium into MoS_2 has been previously reported using calcium in liquid ammonia to yield the superconducting phase $Ca_{0.2}(NH_3)_{0.17}MoS_2$ with a maximal T_c of 8.6 K.[14] As one of only a small handful of materials known to undergo reductive intercalation of calcium and in doing so affording nontrivial changes in the phase's electronic structure, MoS_2 was identified as an ideal material for evaluating calcium

View Article Online
DOI: 10.1039/D5TA09290F

pyrenide as a reductant. Relative to monovalent cations, strong solvation of divalent cations like Ca^{2+} makes the extent and reversibility of insertion into a host lattice particularly solvent sensitive. Additionally, there is a likelihood of the co-insertion of solvent molecules, and an unusual Ca^{2+} coordination environment as a partial solvate also impacting the reactivity and properties of the product phases.

To confirm the incorporation of calcium in reduced MoS_2, scanning electron microscopy (SEM) coupled with energy-dispersive X-ray spectroscopy (EDX) was performed on the calcium-reduced MoS_2 samples. Elemental mapping showed a qualitatively uniform distribution of the elements Ca, Mo, and S throughout each sample, as shown in **Supplementary Figures S15–S20 and Tables S4–S6**. By EDX, calcium content increased with the reaction stoichiometry's quantity of Ca added, **Table 1**. However, large statistical uncertainties inherent to how EDX spectra are collected yield only very approximate element ratios. Precise chemical compositions of the bulk powders were determined using a combination of inductively coupled plasma-optical emission spectroscopy (ICP-OES) to determine the relative concentrations of Ca, Mo, and S in the dissolved products and thermogravimetric analysis (TGA) to estimate the quantity of co-intercalated DMF, **Supplementary Figures S21–S23**. Summarized in **Table 1**, the measured calcium content increases with the reactant stoichiometry's quantity of calcium. A maximal extent of reduction under these conditions was determined to be $Ca_{0.34}(DMF)_{0.20}MoS_{1.94}$, formed by reacting MoS_2 with 0.7 equivalents of calcium pyrenide. By TGA, approximately one-half an equivalent of DMF was found to co-intercalate into the calciation products with each equivalent of calcium.

Table 1. Theoretical and measured element ratios in prepared $Ca_x(DMF)_yMoS_2$ samples calculated using ICP-OES and TGA. A local sample of atom ratios measured by EDX are shown for comparison.

Equiv. Ca added	Empirical formula (ICP-OES, TGA)	Atom ratios† (SEM/EDX)
0.3	$Ca_{0.21}(DMF)_{0.11}MoS_{2.04}$	$Ca_{0.42}MoS_{2.4}$
0.5	$Ca_{0.32}(DMF)_{0.17}MoS_{1.99}$	$Ca_{0.54}MoS_{2.2}$
0.7	$Ca_{0.34}(DMF)_{0.20}MoS_{1.94}$	$Ca_{0.86}MoS_{2.9}$

†Approximate estimate from sampling (~1 μm²).

To this end, 0.3, 0.5, and 0.7 equivalents of calcium pyrenide in DMF, quantified by moles of Ca (*s*) used in preparation of the calcium pyrenide solution, were mixed with MoS_2 at room temperature and stirred overnight. The resulting product was isolated by filtration and analyzed using air-free PXRD, **Figure 4**. In the layered MoS_2, which crystallizes in a hexagonal crystal system, the 2D layers lie normal to the *c*-axis. With increasing extents of reduction, those reflections with non-zero *l* indices diminish monotonically and new reflections at diffraction angles below the (0 0 2) of the parent MoS_2 emerge at $2\theta = 4.5°$, 8.4°, and 12.5°. All the while, the (1 0 0) and (1 1 0) remain essentially unchanged. This observation is consistent with a lattice expansion along the *c*-axis and a distribution of stagings in the resulting intercalated MoS_2. Similar structural transformations have also been reported for $Ca_x(NH_3)_yMoS_2$, where attenuation of the same MoS_2 reflections and emergence of new low-angle peaks were also noted.[14] Owing to the difference in co-intercalated solvent, the number and positions of the new low-angle reflections are evidently also different. No change in the PXRD was observed after stirring the MoS_2 in pure DMF overnight, **Supplementary Figure S24**.

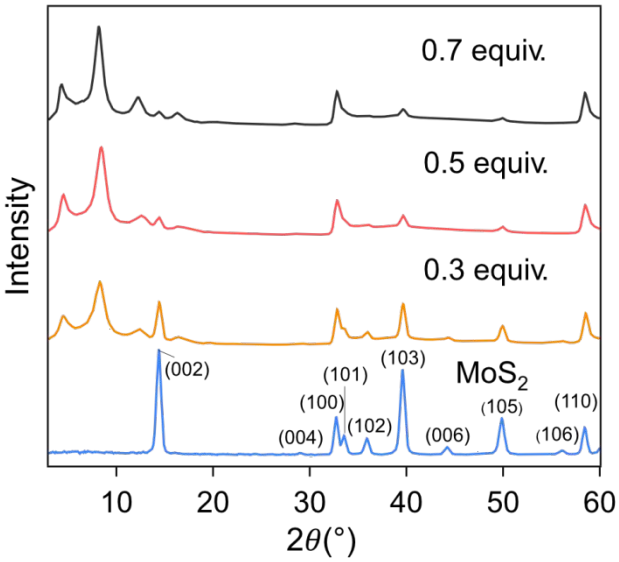

Figure 4. PXRD pattern (λ = 1.54184 Å) for pristine MoS_2 (blue), and 0.3 (yellow), 0.5 (red), and 0.7 (black) equivalents of $Ca(pyrene)_2$ used to perform Ca reductive insertion on MoS_2.

CONCLUSIONS

Convenient methods for stoichiometric calciation provide opportunities for synthesis, including access to reduced coordination compounds charge-balanced by calcium, facile screening of potential calcium-ion insertion materials for potential energy storage applications, controlled polaron injection using divalent cations, and other solid-state chemical transformations. Here, chemiluminescent reduction of pyrene by calcium metal was observed to serve as a competent room-temperature stoichiometric reductant with a potential of –2.52 V vs $Fc^{+1/0}$. Owing to the dispersal of fine calcium powder upon the formation of calcium pyrenide, solutions with greater than two equivalents of pyrene to calcium in DMF were found to be ideal for formation of the homogeneous solution-phase reductant. Single crystals of calcium pyrenide with the tentative formula $Ca(THF)_6(pyrene)_2(pyrenide^{\bullet-})_2$ were grown, with bond lengths of the pyrenide ions consistent with those of previously reported single crystals of sodium salts of the pyrene radical anion. In solution, the species was observed to be EPR active, though the UV–*vis* absorption spectra were found most consistent with previous reports of alkali metal salts of the pyrenide dianion. These results may suggest comproportionation of pyrene and pyrenide occurring upon crystallization. Finally, calcium pyrenide solutions in DMF demonstrated reductive calciation of MoS_2 as an illustrative example of the reagent's utility in evaluating potential calcium ion insertion materials at room temperature.

ASSOCIATED CONTENT

Supporting Information

The Supporting Information is available free of charge on the RSC Publications website.

- Supplementary Information including PXRD, EPR, and NMR data (PDF)
- Video of the calcium reduction reaction (mp4)

View Article Online
DOI: 10.1039/D5TA09290F

AUTHOR INFORMATION

Corresponding Author

* Michael L. Aubrey (michael.aubrey@austin.utexas.edu).

Author Contributions

A. Wang and R. Storteboom conducted the experiments, S. S. Mollick initiated the project and conducted the SEM images analyses, and M. L. Aubrey designed the experiments and directed the project. All co-authors contributed to the completion of the manuscript.

ACKNOWLEDGMENT

We gratefully acknowledge the UT Austin Department of Chemistry's X-ray Diffraction Facility for experimental and analytical assistance, and Dr. Scott Smith, director of the University of Texas at Austin Nuclear Magnetic Resonance Lab, for his assistance collecting the reported EPR spectra.

REFERENCES

(1) Whittingham, M. S. Electrical Energy Storage and Intercalation Chemistry. *Science* **1976**, *192* (4244), 1126–1127. https://doi.org/10.1126/science.192.4244.1126.

(2) Yoshino, A. The Birth of the Lithium-Ion Battery. *Angew. Chemic Int. Edit.* **2012**, *51* (24), 5798–5800. https://doi.org/10.1002/anie.201105006.

(3) Mizushima, K.; Jones, P. C.; Wiseman, P. J.; Goodenough, J. B. Li_xCoO_2 ($0 < x < -1$): A New Cathode Material for Batteries of High Energy Density. *Mater Res. Bull.* **1980**, *15* (6), 783–789. https://doi.org/10.1016/0025-5408(80)90012-4.

(4) Starnberg, H. I.; Brauer, H. E.; Holleboom, L. J.; Hughes, H. P. 3D-to-2D Transition by Cs Intercalation of VSe_2. *Phys. Rev. Lett.* **1993**, *70* (20), 3111–3114. https://doi.org/10.1103/PhysRevLett.70.3111.

(5) Hebard, A. F.; Rosseinsky, M. J.; Haddon, R. C.; Murphy, D. W.; Glarum, S. H.; Palstra, T. T. M.; Ramirez, A. P.; Kortan, A. R. Superconductivity at 18 K in Potassium-Doped C_{60}. *Nature* **1991**, *350* (6319), 600–601. https://doi.org/10.1038/350600a0.

(6) Friend, R. H.; Yoffe, A. D. Electronic Properties of Intercalation Complexes of the Transition Metal Dichalcogenides. *Adv. Phys.* **1987**, *36* (1), 1–94. https://doi.org/10.1080/00018738700101951.

(7) Liang, Y.; Dong, H.; Aurbach, D.; Yao, Y. Current Status and Future Directions of Multivalent Metal-Ion Batteries. *Nat. Energy* **2020**, *5* (9), 646–656. https://doi.org/10.1038/s41560-020-0655-0.

(8) Maroni, F.; Dongmo, S.; Gauckler, C.; Marinaro, M.; Wohlfahrt-Mehrens, M. Through the Maze of Multivalent-Ion Batteries: A Critical Review on the Status of the Research on Cathode Materials for Mg^{2+} and Ca^{2+} Ions Insertion. *Batteries & Supercaps* **2021**, *4* (8), 1221–1251. https://doi.org/10.1002/batt.202000330.

(9) Franchini, C.; Reticcioli, M.; Setvin, M.; Diebold, U. Polarons in Materials. *Nat Rev Mater* **2021**, *6* (7), 560–586. https://doi.org/10.1038/s41578-021-00289-w.

(10) Bratsch, S. G. Standard Electrode Potentials and Temperature Coefficients in Water at 298.15 K. *J. Phys. Chem. Ref. Data* **1989**, *18* (1), 1–21. https://doi.org/10.1063/1.555839.

(11) Kuperman, N.; Padigi, P.; Goncher, G.; Evans, D.; Thiebes, J.; Solanki, R. High Performance Prussian Blue Cathode for Nonaqueous Ca-Ion Intercalation Battery. *J. Power Sources* **2017**, *342*, 414–418. https://doi.org/10.1016/j.jpowsour.2016.12.074.

(12) Jeon, B.; Heo, J. W.; Hyoung, J.; Kwak, H. H.; Lee, D. M.; Hong, S.-T. Reversible Calcium-Ion Insertion in NASICON-Type $NaV_2(PO_4)_3$. *Chem. Mater.* **2020**, *32* (20), 8772–8780. https://doi.org/10.1021/acs.chemmater.0c01112.

(13) Tchitchekova, D. S.; Ponrouch, A.; Verrelli, R.; Broux, T.; Frontera, C.; Sorrentino, A.; Bardé, F.; Biskup, N.; Arroyo-de Dompablo, M. E.; Palacín, M. R. Electrochemical Intercalation of Calcium and Magnesium in TiS_2: Fundamental Studies Related to Multivalent Battery Applications. *Chem. Mater.* **2018**, *30* (3), 847–856. https://doi.org/10.1021/acs.chemmater.7b04406.

(14) Zhou, M.; Li, X.; Yang, L.; Dong, C. Synthesis, Crystal Structure and Superconducting Properties of Calcium Intercalates of MoS_2. *J. Solid State Chem.* **2018**, *258*, 131–137. https://doi.org/10.1016/j.jssc.2017.10.015.

(15) Cabello, M.; Nacimiento, F.; González, J. R.; Ortiz, G.; Alcántara, R.; Lavela, P.; Pérez-Vicente, C.; Tirado, J. L. Advancing towards a Veritable Calcium-Ion Battery: $CaCo_2O_4$ Positive Electrode Material. *Electrochem. Commun.* **2016**, *67*, 59–64. https://doi.org/10.1016/j.elecom.2016.03.016.

(16) Tojo, T.; Tawa, H.; Oshida, N.; Inada, R.; Sakurai, Y. Electrochemical Characterization of a Layered α-MoO_3 as a New Cathode Material for Calcium Ion Batteries. *J. Electroanal. Chem.* **2018**, *825*, 51–56. https://doi.org/10.1016/j.jelechem.2018.08.008.

(17) Hayashi, M.; Arai, H.; Ohtsuka, H.; Sakurai, Y. Electrochemical Insertion/Extraction of Calcium Ions Using Crystalline Vanadium Oxide. *Electrochem. Solid-State Lett.* **2004**, *7* (5), A119. https://doi.org/10.1149/1.1675951.

(18) Connelly, N. G.; Geiger, W. E. Chemical Redox Agents for Organometallic Chemistry. *Chem. Rev.* **1996**, *96* (2), 877–910. https://doi.org/10.1021/cr940053x.

(19) Au, H.; Rubio, N.; Buckley, D. J.; Mattevi, C.; Shaffer, M. S. P. Thermal Decomposition of Ternary Sodium Graphite Intercalation Compounds. *Chem. Euro. J.* **2020**, *26* (29), 6545–6553. https://doi.org/10.1002/chem.202000422.

(20) Biggins, N.; Ziebel, M. E.; Gonzalez, M. I.; Long, J. R. Crystallographic Characterization of the Metal–Organic Framework $Fe_2(Bdp)_3$ upon Reductive Cation Insertion. *Chem. Sci.* **2020**, *11* (34), 9173–9180. https://doi.org/10.1039/D0SC03383A.

(21) Näther, C.; Bock, H.; Claridge, R. F. C. Solvent-shared Radical Ion Pairs [Pyrene$^{\cdot\ominus}$Na$^{\oplus}$ $(C_2H_5)_2]_\infty$%: ESR Evidence for Two Different Aggregates in Solution, Room Temperature Crystallization, and Structural Proof of Another Polymorphic Modification. *Helv. Chimica Acta* **1996**, *79* (1), 84–91. https://doi.org/10.1002/hlca.19960790109.

(22) Liu, Z.; Lunchev, A. V.; Li, W.; Ruan, S.; Yazami, R.; Grimsdale, A. C.; Su, H. Electrochemical Properties of

View Article Online
DOI: 10.1039/D5TA09290F

Anthracene-Based Lithium-Solvated Electron Solutions. *ACS Omega* **2019**, *4* (3), 4707–4711. https://doi.org/10.1021/acsomega.8b03621.

(23) Bock, H.; Arad, C.; Näther, C.; Havlas, Z. The Structures of Solvent-Separated Naphthalene and Anthracene Radical Anions. *J. Chem. Soc., Chem. Commun.* **1995**, *0* (23), 2393–2394. https://doi.org/10.1039/C39950002393.

(24) Scott, N. D.; Walker, J. F.; Hansley, V. L. Sodium Naphthalene. I. A New Method for the Preparation of Addition Compounds of Alkali Metals and Polycyclic Aromatic Hydrocarbons. *J. Am. Chem. Soc.* **1936**, *58* (12), 2442–2444. https://doi.org/10.1021/ja01303a022.

(25) Melero, C.; Guijarro, A.; Yus, M. Structural Characterization and Bonding Properties of Lithium Naphthalene Radical Anion, $[Li^+(TMEDA)_2][C_{10}H_8^{\cdot -}]$, and Lithium Naphthalene Dianion $[(Li^+TMEDA)_2C_{10}H_8^{-2}]$. *Dalton Trans.* **2009**, No. 8, 1286. https://doi.org/10.1039/b821119c.

(26) Scott, T. A.; Ooro, B. A.; Collins, D. J.; Shatruk, M.; Yakovenko, A.; Dunbar, K. R.; Zhou, H.-C. After 118 Years, the Isolation of Two Common Radical Anion Reductants as Simple, Stable Solids. *Chem. Commun.* **2009**, No. 1, 65–67. https://doi.org/10.1039/B815272A.

(27) Sheldrick, G. M. SHELXT – Integrated Space-Group and Crystal-Structure Determination. *Acta Cryst. A* **2015**, *71* (1), 3–8. https://doi.org/10.1107/s2053273314026370.

(28) Sheldrick, G. M. Crystal Structure Refinement with SHELXL. *Acta Cryst. C* **2015**, *71* (1), 3–8. https://doi.org/10.1107/s2053229614024218.

(29) Dolomanov, O. V.; Bourhis, L. J.; Gildea, R. J.; Howard, J. A. K.; Puschmann, H. OLEX2: A Complete Structure Solution, Refinement and Analysis Program. *J. Appl. Crystalogr.* **2009**, *42* (2), 339–341. https://doi.org/10.1107/s0021889808042726.

(30) Momma, K.; Izumi, F. *VESTA 3* for Three-Dimensional Visualization of Crystal, Volumetric and Morphology Data. *J. Appl. Crystallogr.* **2011**, *44* (6), 1272–1276. https://doi.org/10.1107/S0021889811038970.

(31) Weller, A.; Zachariasse, K. Chemiluminescence from Chemical Oxidation of Aromatic Anions. *J. Chem. Phys.* **1967**, *46* (12), 4984–4985. https://doi.org/10.1063/1.1840667.

(32) Maloy, J. T.; Prater, K. B.; Bard, A. J. Electrogenerated Chemiluminescence. II. The Rotating Ring-Disk Electrode and the Pyrene-N,N,N',N'-Tetramethyl-p-Phenylenediamine System. *J. Phys. Chem.* **1968**, *72* (12), 4348–4350. https://doi.org/10.1021/j100858a084.

(33) Pang, X.; Wang, H.; Wang, W.; Jin, W. J. Phosphorescent π-Hole···π Bonding Cocrystals of Pyrene with Halo-Perfluorobenzenes (F, Cl, Br, I). *Cryst. Growth & Design* **2015**, *15* (10), 4938–4945. https://doi.org/10.1021/acs.cgd.5b00844.

(34) Eichstaedt, N.; Pietsch, I.; Friedrich, D.; Breu, J. Polycyclic Aromatic Hydrocarbon Radical Anions Stabilized by a Sodium Diglyme Cation Complex. *Z. anorg. allge. chemie* **2023**, *649* (24), e202300168. https://doi.org/10.1002/zaac.202300168.

(35) Rozenshtein, V.; Zilber, G.; Rabinovitz, M.; Levanon, H. Irregular Photoinduced Electron Transfer between Pyrene Dianion and Alkali Metal Cations Studied by Fourier-Transform Electron Paramagnetic Resonance. *J. Am. Chem. Soc.* **1993**, *115* (12), 5193–5203. https://doi.org/10.1021/ja00065a035.

(36) Bruyers, D. K. F.; Richert, S. Design of an Electrochemical Cell for Continuous Wave EPR Measurements of Radical Ions. *Chem. Euro. J.* **2024**, *30* (69), e202402719. https://doi.org/10.1002/chem.202402719.

(37) Koláčná, L.; Klíma, J.; Polák, P.; Tobrman, T.; Liška, A.; Ludvík, J. Electrochemical, EPR, and Computational Study of Pyrene Conjugates—Precursors for Novel Type of Organic Semiconductors. *J. Solid State Electrochem.* **2022**, *26* (2), 503–514. https://doi.org/10.1007/s10008-021-05094-7.

(38) Tsierkezos, N. G. Cyclic Voltammetric Studies of Ferrocene in Nonaqueous Solvents in the Temperature Range from 248.15 to 298.15 K. *J. Solution Chem.* **2007**, *36* (3), 289–302. https://doi.org/10.1007/s10953-006-9119-9.

(39) Bond, A. M.; Oldham, K. B.; Snook, G. A. Use of the Ferrocene Oxidation Process To Provide Both Reference Electrode Potential Calibration and a Simple Measurement (via Semiintegration) of the Uncompensated Resistance in Cyclic Voltammetric Studies in High-Resistance Organic Solvents. *Anal. Chem.* **2000**, *72* (15), 3492–3496. https://doi.org/10.1021/ac000020j.

(40) Intercalation Chemistry of Metal Chalcogenohalide. In *Intercalation chemistry*; Whittingham, M. S., Jacobson, A. J., Eds.; Materials science and technology; Academic Press: New York, 1982; pp 375–401.

(41) Fan, X.; Xu, P.; Zhou, D.; Sun, Y.; Li, Y. C.; Nguyen, M. A. T.; Terrones, M.; Mallouk, T. E. Fast and Efficient Preparation of Exfoliated 2H MoS_2 Nanosheets by Sonication-Assisted Lithium Intercalation and Infrared Laser-Induced 1T to 2H Phase Reversion. *Nano Lett.* **2015**, *15* (9), 5956–5960. https://doi.org/10.1021/acs.nanolett.5b02091.

(42) Py, M. A.; Haering, R. R. Structural Destabilization Induced by Lithium Intercalation in MoS_2 and Related Compounds. *Can. J. Phys.* **1983**, *61* (1), 76–84. https://doi.org/10.1139/p83-013.

(43) Voiry, D.; Mohite, A.; Chhowalla, M. Phase Engineering of Transition Metal Dichalcogenides. *Chem. Soc. Rev.* **2015**, *44* (9), 2702–2712. https://doi.org/10.1039/C5CS00151J.

View Article Online
DOI: 10.1039/D5TA09290F

View Article Online
DOI: 10.1039/D5TA09290F

Data availability

The data supporting this article have been included as part of the Supplementary Information. Crystallographic data has been deposited at the CCDC under the deposition number 2489905.